MAX meets ADAM: A dosimetric comparison between a voxel-based and a mathematical model for external exposure to photons

R Kramer[1] , J W Vieira[1] , H J Khoury[1] and F de Andrade Lima[2]

[1] Departamento de Energia Nuclear, Universidade Federal de Pernambuco, Recife,PE,Brazil

[2] Centro Regional de Ciências Nucleares, Recife,PE,Brazil

E-mail: rkramer@uol.com.br

Statement of provenance:
'This is an author-created, un-copyedited version of an article accepted for publication in Physics in Medicine and Biology. IOP Publishing Ltd is not responsible for any errors or omissions in this version of the manuscript or any version derived from it. The definitive publisher authenticated version is available at DOI: 10.1088/0031-9155/49/6/002. '

Abstract

The International Commission on Radiological Protection (ICRP) intends to revise the organ and tissue equivalent dose conversion coefficients published in various reports. For this purpose the mathematical human MIRD phantoms, actually in use, have to be replaced by recently developed voxel-based phantoms. This study investigates the dosimetric consequences, especially with respect to the effective male dose, if not only a MIRD phantom is replaced by a voxel phantom, but also if the tissue compositions, and the radiation transport codes are changed. This task will be resolved by systematically replacing in the mathematical ADAM/GSF exposure model, first the radiation transport code, then the tissue composition, and finally the phantom anatomy, in order to arrive at the voxel-based MAX/EGS4 exposure model. The results show that the combined effect of these replacements can decrease the effective male dose by up to 25% for external exposures to photons for incident energies above 30 keV for different field geometries, mainly because of increased shielding by a heterogeneous skeleton and by overlying adipose and muscle tissue, and also because of the positions internal organs have in a realistically designed human body compared to their positions in the mathematically constructed phantom.

1. Introduction

In its 2001 Annual Report (ICRP 2002) the International Commission on Radiological Protection (ICRP) outlines the activities of its various committees and task groups. With regard to the objectives of the task group on 'Dose Calculation' the report puts on record:
"….. The aim is to replace the current MIRD phantoms, which are based on simple geometric shapes of organs and tissues, with more realistic representations of organs and tissues based upon medical imaging data. These new phantoms are expected to be developed from voxel (volume pixel) phantoms in which the body can be represented by many millions of voxels each identified as a particular tissue type."
While the MIRD phantoms are composed of mathematically defined organs, voxel-based phantoms, or simply voxel phantoms, are based on digital images recorded from scanning of real persons by computed tomography (CT) or magnetic resonance imaging (MRI). Compared to mathematical phantoms they are true to nature representations of a human body.

The replacement of the mathematical MIRD phantoms by voxel-based models is the precondition for the re-calculation of equivalent dose conversion coefficients (CCs) published by the ICRP for external as well as for internal exposures (ICRP 1994, 1996).
CCs are ratios between equivalent dose to organs and tissues at risk (protection quantities) and measurable or operational quantities, which have been determined by use of exposure models. An exposure model is a physical or computational arrangement for the simultaneous determination of protection and operational quantities for exposure conditions relevant in radiation protection. It must therefore incorporate sources and fields of the radiations involved, a model of the human body with respect to tissue composition and organ anatomy, and a method for the determination of equivalent dose inside the human body, and of the operational quantities of interest.

Since the beginning of the voxel phantom development comparisons have been made with CCs calculated for the MIRD phantoms.
Such studies have been published for external and internal exposures to photons or electrons
- by Jones (1995, 1997, 1998), Hunt et al (2000) and Dantas et al (2001) for the NORMAN voxel phantom (Dimbylow 1995),
- by Petoussi-Henss et al (1997, 1998, 2002), Smith et al (2000, 2001), and Zankl et al (2000, 2002) for the GSF voxel phantoms (Zankl and Wittman 2001, Petoussi-Henss et al 2002),
- by Tagesson et al (1995), Petoussi-Henss (1998), Zankl et al (2000), Hunt et al (2000), Yoriyaz and Stabin (2000), and Stabin and Yoriyaz (2002) for the VOXELMAN phantom (Zubal et al 1994),
- by Chao et al (2001a), Chao et al (2001b), and Xu and Chao (2003) for the VIPMAN voxel phantom (Xu et al 2000),
- and by Saito et al (2001) for the OTOKO voxel phantom.

There seems to be general agreement that differences between organ masses, and between the positions of organs can explain the differences found between the CCs for the phantoms considered. However, these conclusions were often made without considering the influence of different tissue compositions and of different radiation transport methods, thereby suggesting that the equivalent dose differences found were caused only by the differences of the anatomy.
The CCs for adults for external exposure to photons recommended by the ICRP (ICRP 1996) have been calculated with an exposure model composed of the GSF Monte Carlo code (Kramer 1979, Zankl et al 1997), of body tissue compositions which had been taken from an early MIRD publication (Snyder et al 1969), and from ICRP Report 23 (ICRP 1975), and of the mathematical, gender-specific MIRD-type phantoms, called ADAM and EVA (Kramer et al 1982).
Meanwhile, apart from the voxel phantom development, progress has been made in the development of new radiation transport codes, like the EGS4 Monte Carlo code (Nelson et al 1985), the MCNP4 Monte Carlo code (Briesmeister 1997), and the PENELOPE Monte Carlo code (Baro et al 1995), which allow for the coupled transport of photons and electrons based on the increased speed of modern computers, and tissue compositions for the human body have been revised by the International Commission on Radiation Units and Measurements in its Report No.44 (ICRU 1989).
This investigation will examine the change of CCs for a male adult person externally exposed to photons if the existing mathematical ADAM/GSF exposure model is replaced by the voxel-based MAX/EGS4 exposure model, which has been introduced recently by Kramer et al (2003). The task will be carried out in three steps:

1. Replacement of the GSF Monte Carlo code by the EGS4 Monte Carlo code for the mathematical ADAM phantom.
2. Replacement of the existing tissue compositions of the ADAM phantom by compositions based on data recommended by ICRU44.
3. Replacement of the mathematical ADAM phantom by the voxel-based MAX phantom.

2. Materials and methods

2.1 Organs and tissues at risk

The basic dosimetric quantity related to the probability of appearance of stochastic radiation effects as defined by the International Commission on Radiological Protection (ICRP) is the effective dose, which "is the sum of the weighted equivalent doses in all tissues and organs of the body. It is given by the expression

$$E = \sum_T w_T H_T$$

where H_T is the equivalent dose in tissue or organ T and w_T is the weighting factor for tissue T " (ICRP 1991). The Commission recommends weighting factors for 13 tissues and organs, among which the 'gonads' represent the testes as well as the ovaries, and 'bone surface' the osteogenic cells on the endosteal surface of bone, plus for a so-called 'remainder', which is composed of another 10 organs and tissues as shown in table 1.

Table 1. Tissue weighting factors as defined by ICRP60.

Tissue/organ	Tissue weighting factors (w_T)
Gonads	0.20
RBM	0.12
Colon	0.12
Lung	0.12
Stomach	0.12
Bladder	0.05
Breast	0.05
Liver	0.05
Oesophagus	0.05
Thyroid	0.05
Skin	0.01
Bone surface	0.01
Remainder	0.05

RBM = Red bone marrow

In order to understand how the replacement of the MIRD phantoms by voxel phantoms may influence the effective dose, one has to compare the equivalent doses for the organs and tissues mentioned in table 1 for the two types of models for a given exposure situation.

As a female voxel phantom was not available for this investigation, it was decided to calculate an effective male dose. For this purpose the breasts, the ovaries and the uterus have been left out from the list of organs and tissues mentioned in table 1. The tissue weighting factors have not been re-normalized which means that their sum is 0.95. The gonad weighting factor of 0.2 was applied to the equivalent dose to the testes, and the remainder consisted of only 9 organs instead of 10.

2.2 The mathematical ADAM/GSF exposure model

The mathematical ADAM phantom was introduced by Kramer et al (1982) as a gender-specific derivative of the hermaphrodite MIRD5 phantom (Snyder et al 1974). The form of the body and its organs are described by mathematical expressions representing planes, circular and elliptical cylinders, spheres, cones, tori, etc., and combinations and intersections thereof. Organ masses, body weight and body height correspond to the anatomical data recommended in the first ICRP Reference Man Report, ICRP Publication No. 23 (ICRP 1975).

Figure 1 shows a lateral and frontal view of the ADAM phantom with 17 of the 21 male organs and tissues at risk. All organs have been visualized based on the mathematical expressions given in Kramer et al (1982), except for the addition of the trachea based on data from anatomical textbooks, and except for the omission of the 'genitalia region', which was introduced in the original version of the ADAM phantom to improve the coefficient of variance for the equivalent dose to the testes. Figure 2 represents an abdominal cross-section through the ADAM phantom.
Connected to the GSF Monte Carlo code (Kramer 1979, Zankl et al 1997), the ADAM phantom was widely used to calculate kerma-approximated CCs for external exposures to photons for applications in medical, occupational, and environmental radiation protection.
The GSF code uses a non-analog Monte Carlo method, which applies the same photon transport physics as the ALGAM code (Warner and Craig 1968), the so-called fractional photon technique, in order to increase the number of photon scattering events in deeply penetrated areas of the phantoms body, thereby reducing the coefficient of variance. Rayleigh scattering and secondary electrons are not considered by this code. The photon cross-section data were taken from Roussin et al (1983).

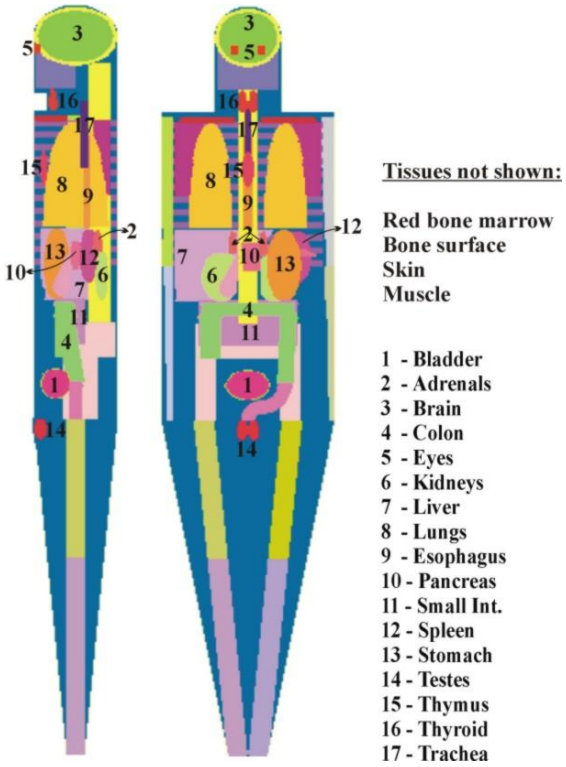

Figure 1. Male adult mathematical ADAM phantom: Lateral and frontal view

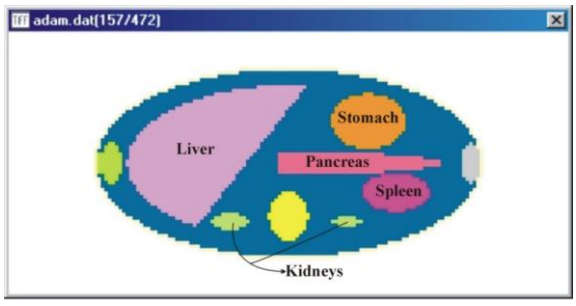

Figure 2. Male adult mathematical ADAM phantom: Abdominal cross-section

2.3 The voxel-based MAX/EGS4 exposure model

The MAX (Male Adult voXel) phantom was introduced by Kramer et al (2003) as the first human phantom which corresponds to the male anatomical data of the second ICRP Reference Man Report, Publication No. 89 (ICRP 2003), for most organs and tissues at risk. This voxel phantom is based on digital images recorded from scanning of a patient by computed tomography and magnetic resonance imaging (Zubal 1994). The patient's body height was 175 cm, which is only 1cm less than the male reference height.
Figure 3 shows a frontal view, and figure 4 a lateral view of the MAX phantom with 17 of the 21 male organs and tissues at risk. For the sake of clearness the skeleton is shown in separate images.
An abdominal cross-section through the MAX phantom can be seen in figure 5.

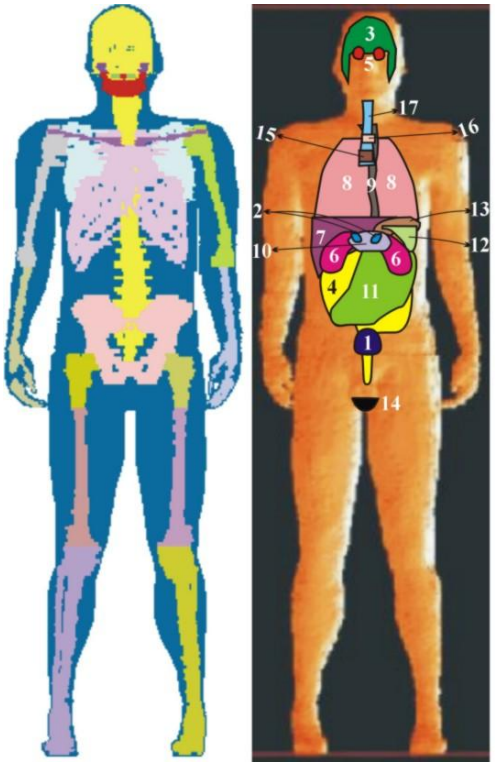

Figure 3. MAX phantom: frontal views of the skeleton and of the internal organs

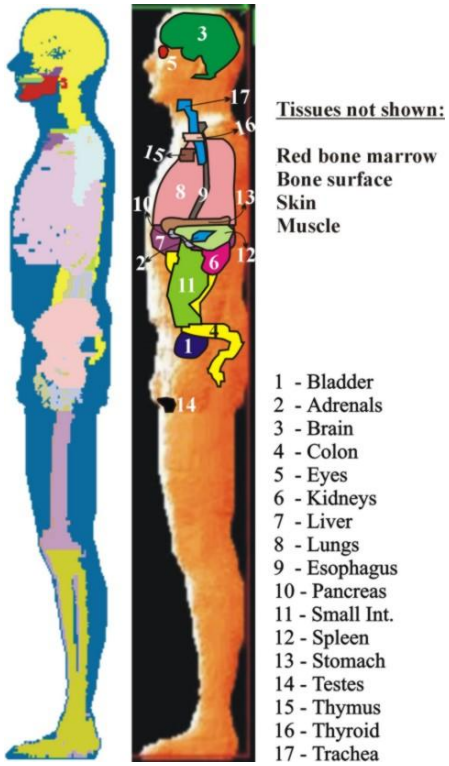

Figure 4. MAX phantom: lateral views of the skeleton and of the internal organs

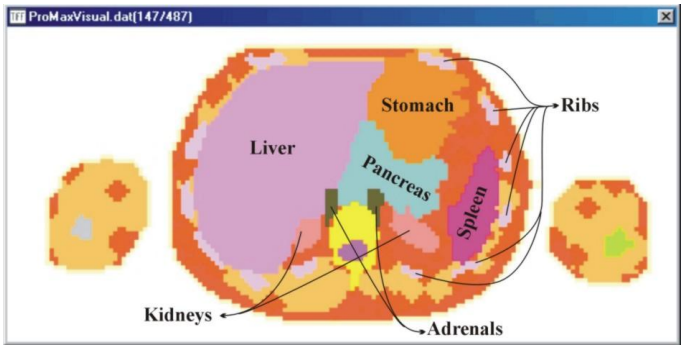

Figure 5. MAX phantom: Abdominal cross-section

The MAX phantom is connected to the EGS4 Monte Carlo code (Nelson et al 1985), which simulates coupled electron-photon transport through arbitrary media. The default version of EGS4 applies an analog Monte Carlo method, which was used for the calculations of this investigation. Rayleigh scattering and secondary electrons have normally been taken into account in the calculations. The photon cross-sections were taken from Storm and Israel (1970) and from Hubbell and Overbo (1979).

2.4 Organ masses and tissue composition

The organ and tissue masses of the ADAM phantom correspond to the data specified by ICRP in its first Reference Man report, Publication No.23 (ICRP 1975). These data have been revised and published in Publication No.89 (ICRP 2003). The organ and tissue masses of the MAX phantom

correspond to the ICRP89 data. A detailed description and comparison for the organ and tissue masses of the two phantoms can be found in Kramer et al (2003).

Table 2. Elemental mass fractions for the ADAM and the ADAM44 phantom

ATOM	SOFT ADAM44 [%]	SOFT ADAM [%]	SKIN ADAM44 [%]	SKIN ADAM [%]	LUNGS ADAM44 [%]	LUNGS ADAM [%]	SKEL. ADAM44 [%]	SKEL. ADAM [%]	ADIMUS ADAM44 [%]
H	10.5	10	10	10.2	10.3	10	7.2	7	10.6
C	12.5	23	20.4	26.9	10.5	10	31.3	23	30.8
N	2.6	2.3	4.2	4.3	3.1	2.8	3.2	3.9	2.4
O	73.5	63	64.5	58	74.9	76	41.1	49	55.4
Na	0.2	0.13	0.2	0.01	0.2	0.2	0.1	0.32	0.1
Mg		0.015		0.005		0.007	0.1	0.11	
P	0.2	0.24	0.1	0.3	0.2	0.08	5.3	6.9	0.128
S	0.18	0.22	0.2	0.15	0.3	0.23	0.25	0.17	0.227
Cl	0.22	0.14	0.3	0.25	0.3	0.27	0.1	0.14	0.1
K	0.21	0.21	0.1	0.1	0.2	0.2	0.05	0.15	0.245
Ca	0.01			0.14		0.007	11.3	9.9	
Fe	0.01	0.006		0.002		0.04		0.008	
ρ [gcm^{-3}]	1.05	0.98	1.09	1.105	0.26	0.296	1.469	(1.486)	1.012

SOFT = Soft tissue, SKEL = Skeleton, ADIMUS = Homogeneous mixture of 36.2% Adipose and 63.8% Muscle

The elemental compositions for the organ and tissues of the ADAM phantom (Kramer et al 1982), shown in table 2, have been taken from the work of Snyder et al (1969), except for the skin whose composition was based on data from ICRP23 (ICRP 1975). Later compositions and densities for the tissues of the MIRD phantoms have been revised by Cristy and Eckerman (1987), which led to a density of 1.4 g cm^{-3} for the homogeneous skeletal mixture compared to the earlier 1.486 g cm^{-3}, although the mass fraction of calcium was increased from 9.9% to 10.19%. Therefore one can conclude that the correct density for the skeletal mixture used in the ADAM phantom actually would have been well below 1.4 g cm^{-3}.
The ADAM phantom with the new ICRU44-based tissue compositions for soft-tissue, the skin, the lungs, adipose, muscle, is called ADAM44 phantom. It has the same soft-tissue compositions as the MAX phantom, except for the ADIMUS mixture. As the ADAM phantom has no separately segmented volumes of adipose and muscle, a homogeneous ADIMUS mixture of 36.2% adipose and 63.8% muscle, which corresponds to the mass ratio of these two tissues in the MAX phantom, will be used in the ADAM44 phantom for all unspecified regions (blue areas in figures 1 and 2). The old skeletal mixture of the ADAM phantom will be replaced in the ADAM44 phantom by a composition which contains 11.3% of calcium, as recommended by ICRP70 (ICRP 1995) for the skeleton of the Reference Adult Male.

The change of the elemental mass fractions of a tissue alters its capacity of absorbing radiation energy, i.e. that among other quantities especially the mass-energy absorption (MEA) coefficient will change. If the MEA coefficient becomes greater, then the equivalent dose to the tissue will increase, and so will the shielding effect for other organs and tissues in the near proximity, and vice versa. For the tissue replacements ADAM→ADAM44 mentioned in table 2, ratios between the ADAM44 and the ADAM MEA coefficients have been calculated and are shown in figure 6 for photon energies from 10 to 200 keV. These data indicate that the replacement of tissue compositions is expected to increase the equivalent dose to soft-tissue organs by up to 9%, to the skeleton by up to 3%, and to the skin by up to 2%, while no significant change would be seen for the lungs. However, the replacement of the ADAM soft-tissue in unspecified regions (blue areas in figures 1 and 2) by the ADAM44 ADIMUS mixture would cause a decrease by up to 7% of the equivalent dose to those regions.

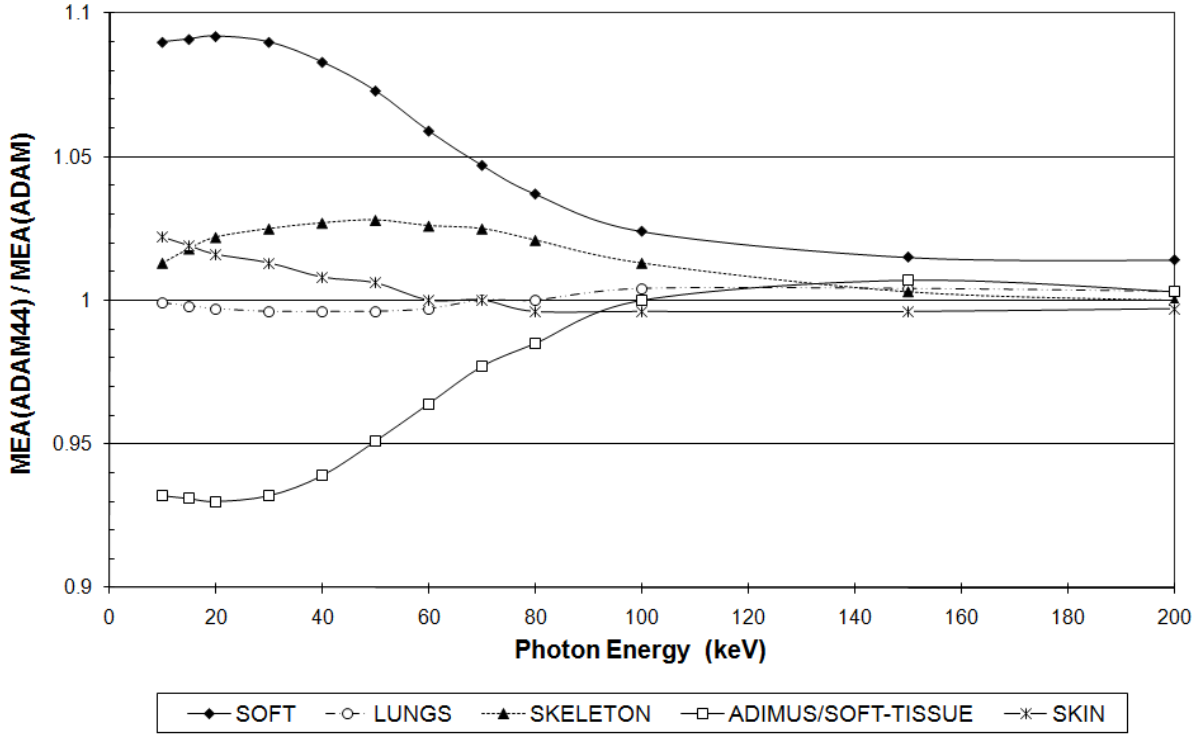

Figure 6. Ratios between mass-energy absorption (MEA) coefficients for body tissues of the ADAM44 and the ADAM phantom

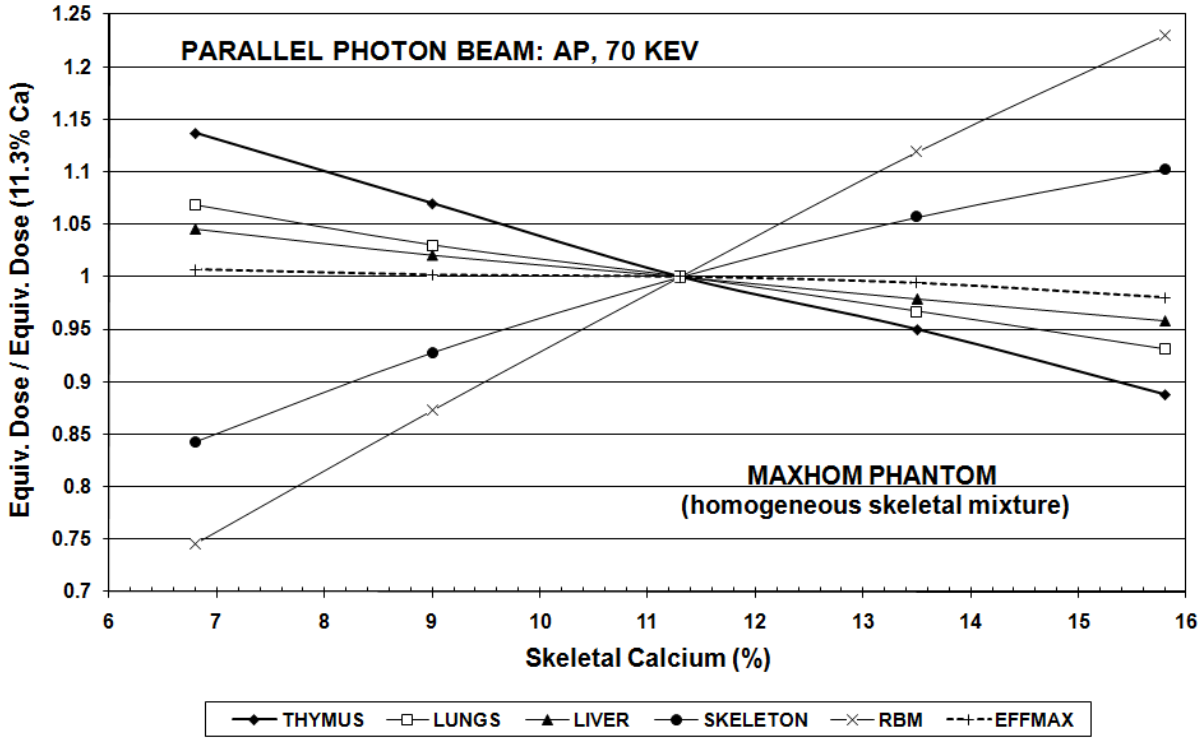

Figure 7. Organ and tissue equivalent doses for the MAXHOM phantom normalized to their value for 11.3% of skeletal calcium as a function of the skeletal calcium content. EFFMAX = effective MAXHOM dose.

The consequences resulting from a change of the content of skeletal calcium can be seen in figure 7. The data have been calculated for a version of the MAX phantom which contains a homogeneous skeleton, they are normalized to the value for the reference calcium content of 11.3% (ICRP 1994), and they are qualitatively valid for any anthropomorphic human phantom. The equivalent doses to the skeleton and to the red bone marrow (RBM) increase with increasing calcium content, while the equivalent doses to underlying organs, like the lungs, the liver and the thymus, and also the effective male dose decrease as a result of the increased shielding, here mainly by the ribcage.

With regard to the replacement of the five tissue compositions ADAM→ADAM44 one can expect

a) that due to the changes of the MEA coefficients the equivalent dose to the soft-tissue organs, the skeleton, and the skin will increase, while the lungs equivalent dose will not change,

b) that the replacement of the soft-tissue in unspecified regions by the ADIMUS mixture will lead to an increase of the equivalent dose to underlying organs and tissues because of reduced shielding, and

c) that the change of the skeletal tissue composition will lead to a decrease of the equivalent dose to underlying organs because of increased shielding.

In the following organ- and tissue-specific discussion these dosimetric results will be referred to as ‘effect A’, ‘effect B’, and ‘effect C’, respectively

2.5 Anatomy

There exist no CT images for the ADAM44 phantom which would allow for the design of a heterogeneous distribution of skeletal tissues as it has been done for the MAX phantom (Kramer et al 2003), and also there exist no separately segmented volumes of adipose and muscle as in the case of the MAX phantom. In order to perform a dosimetric comparison which considers only the anatomical differences between the two phantoms, these two remaining differences with respect to the tissue composition have to be removed. As the ADAM44 phantom cannot be changed for this purpose, i.e. that MAX has to meet ADAM44 half-way. Therefore a phantom called MAXHOM has been derived, based on the following changes introduced into the MAX phantom:

a) The heterogeneous mixture of skeletal tissues was replaced by the homogeneous skeletal mixture of the ADAM44 phantom.
b) All regions of adipose or muscle were replaced by the ADIMUS mixture used in the ADAM44 phantom.

In terms of elemental composition of tissues and their distribution throughout the body the ADAM44 phantom and the MAXHOM phantom are equivalent, and consequently all differences of equivalent doses between these two phantoms are expected to be caused by their different anatomies only.

Figures 1 to 5 demonstrate the most important anatomical differences between the mathematical and the voxel-based phantom:

- While the trunk of ADAM (ADAM44) is a elliptical cylinder with integrated arms and constant thickness of 20 cm sagittal and 40 cm lateral, the MAX phantom’s body thickness varies between 20 to 24 cm sagittal, 50 to 52 cm lateral in the region of the upper arms, and 30 to 33 cm in the abdominal region, where the lower arms and hands are separated from the trunk.
- Compared to the mathematical skeleton of the ADAM (ADAM44) phantom, the natural skeleton of the MAX phantom has a sternum, a quite differently shaped pelvis, and the natural structure of the ribs seem to provide more shielding to internal organs.

- Generally the skeleton and internal organs of the MAX phantom are surrounded by thicker layers of adipose and muscle.
- Certain organs in the ADAM (ADAM44) phantom, like the stomach, the thyroid, and the colon are located too close to the surface.

Consequently one would expect in general most of the organ and tissue equivalent doses of the MAXHOM phantom to be smaller than those determined for the ADAM44 phantom.

Significant equivalent dose differences between MAX and MAXHOM, are expected to be found for the skeleton, and for the RBM, of course, but also for some internal soft-tissue organs which may be affected by skeletal shielding (effect C). The different adipose/muscle distribution between MAX and MAXHOM is dosimetrically not important for the organs and tissues at risk considered here.

3. Results and Discussion

3.1 Exposure conditions and data presentation

CCs between equivalent dose to the male organs and tissues at risk and air kerma free-in-air have been calculated for external whole-body exposures to photons. The directions of incidence for a parallel beam of photons were anterior-posterior (AP), posterior-anterior (PA), left lateral (LLAT), right lateral (RLAT), and a 360^0 rotation around the vertical axis of the phantom (ROT). For each of these exposure geometries CCs have been calculated for 18 incident photon energies between 10 keV and 10 MeV. Secondary electrons have generally also been calculated for energies above 200 keV. For each incident energy 10 Million primary photons have been calculated, except for the 360^0 rotation which has been calculated with 20 Million primaries. Coefficients of variance were usually less than 1%, but for the testes, for the thyroid, and for the esophagus they were 2 – 3%.
However, for incident photon energies below 30 keV coefficients of variance can be significantly greater, especially for small organs, because of low numbers of photon interactions with increasing depth.
For the 11 male organs and tissues from the main list of table 1, plus for the effective male dose the calculations produced 60 CCs. In order to study the dosimetric effects from the replacements of the tissue composition and the phantom anatomy separately, intermediate phantoms, called ADAM44 and MAXHOM, had to be introduced. Consequently the total number of CCs to be presented for the phantoms ADAM, ADAM44, MAXHOM, and MAX would be 240, which is beyond the scope of this paper. While this investigation will present only a small selection of the data produced, the complete data set of CCs will be published on a special website (Kramer et al 2004).

Therefore the following selections have been made:

a) CCs for the testes, the RBM, the lungs, and for the effective male dose will be shown and discussed.
b) According to ICRU57 (ICRU 1998), AP- and ROT-incidence are the irradiation geometries most frequently found in the area of occupational exposures. However, PA-incidence will also be included in the data sets presented.

3.2 Radiation transport methods

In order to apply the radiation transport method of the MAX/EGS4 exposure model to the ADAM phantom, a voxel version of the ADAM phantom was made and connected to the EGS4 Monte Carlo

code, in the same way as it was done for the MAX phantom (Kramer et al 2003). The voxel size was also 0.36cm x 0.36cm x 0.36cm, and the effect of this 'voxelization' on the surfaces of the mathematically defined organs can be seen especially in figure 2.
CCs between equivalent doses to the organs and tissues at risk from table 1 and air kerma free-in-air have been calculated for the ADAM/EGS4 exposure model and compared with corresponding data for the ADAM/GSF exposure model published in GSF-Report 8/97 (Zankl et al 1997), which have also been adopted by ICRP74 (ICRP 1996) and by ICRU57 (ICRU 1998). Secondary electrons and Rayleigh scattering have not been considered for the ADAM/EGS4 calculations in order to ensure correspondence to the ADAM/GSF calculations with regard to the radiation physics simulated. The coefficients of variance for the ADAM/GSF exposure model were 1-2% for the larger organs, like lungs, liver, RBM, etc., and 5-10% for the smaller organs, like the testes, the thyroid, etc.

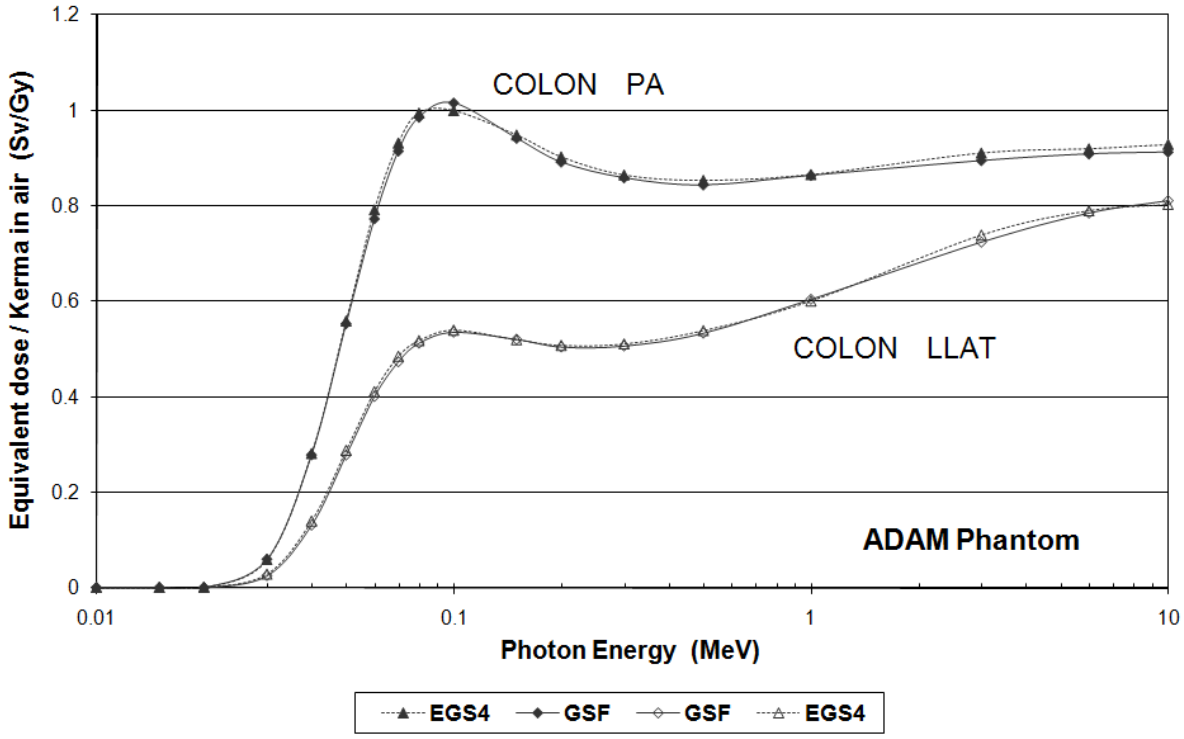

Figure 8. Conversion coefficients for the ADAM phantom between colon equivalent dose and air kerma free-in-air as a function of the incident photon energy for various field geometries and for two different Monte Carlo codes. GSF = GSF Monte Carlo code.

The data comparison between the ADAM/GSF and the ADAM/EGS4 model shows remarkable good agreement in spite of the differences with respect to radiation transport algorithms, photon cross-sections, and random number generators, as can be seen in figure 8 for the colon. Also the 'voxelization' of the smooth surfaces of the organs, especially of the smaller ones, did not change the values of the CCs significantly. This good agreement can be observed throughout the whole set of the calculated CCs, and the differences found between the organ and tissue dose equivalent data of the two exposure models are generally less than 3%, i.e. that the observed differences are well within the margins given by the coefficients of variance of the two models.

3.3 Tissue composition and anatomy

CCs between equivalent dose and air kerma free-in-air as function of the incident photon energy for the 3 selected organs and tissues are shown for AP-, PA-, and ROT-incidence for the ADAM, the ADAM44, the MAXHOM, and the MAX phantom, respectively, in figures 9 to 11.
The dosimetric effects caused by the replacement of the tissue compositions (ADAM→ADAM44), and of the anatomy (ADAM44→MAXHOM), as well as by the inclusion of a heterogeneous skeleton (MAXHOM→MAX) will be discussed for each of the selected organs and tissues.

ADAM→→→ADAM44→→→MAXHOM→→→→→MAX
Composition **Anatomy** **Heterogeneous Skeleton**

The data will show, that compositional shielding, which results from the change of the tissue compositions, and structural shielding, which is caused by the different skeletal anatomies, and the different distribution of adipose and muscle tissue, play an important role for the interpretation of the results.

Testes

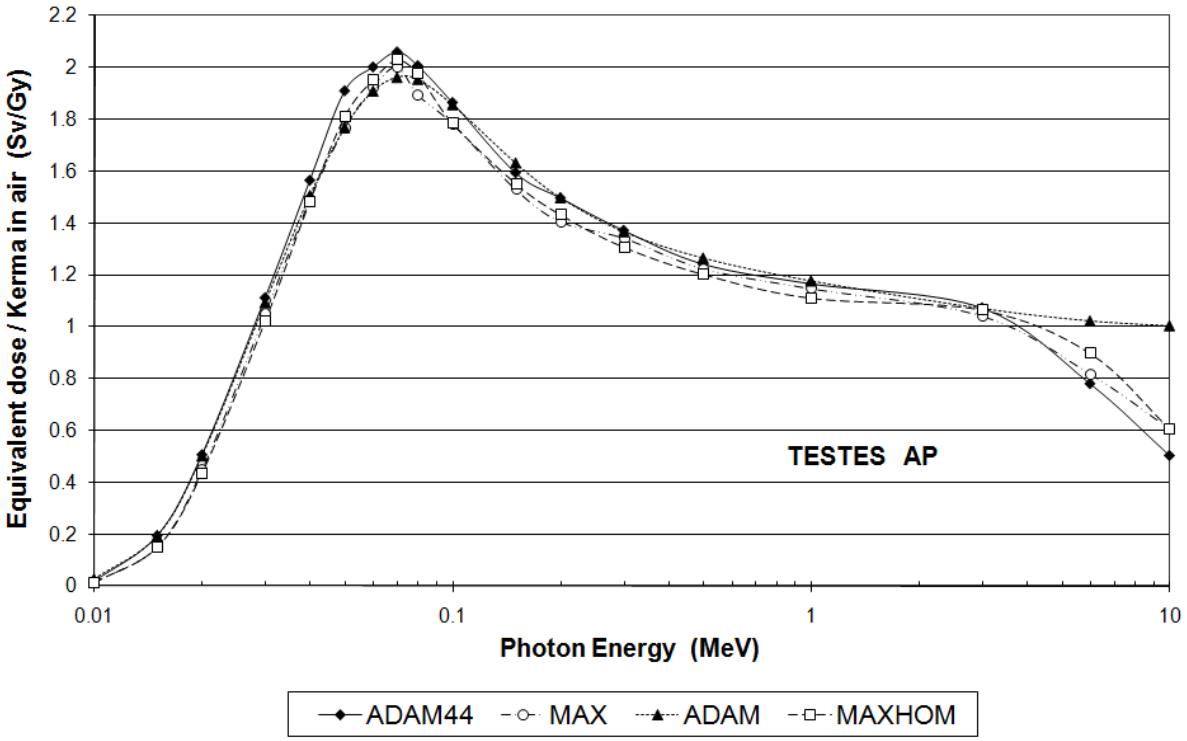

Figure 9a. Conversion coefficients for various phantoms between equivalent dose to the testes and air kerma free-in-air as a function of the incident photon energy for AP-incidence.

Tissue composition (ADAM→ADAM44)
For all direction of incidence shown in figures 9a-c the ADAM44 testes equivalent doses are equal or greater than the corresponding data for ADAM, except for high energies because of the secondary electrons considered in the ADAM44 model. The increase is due to effect A for AP-incidence, and additionally to effect B for PA- and ROT incidence.

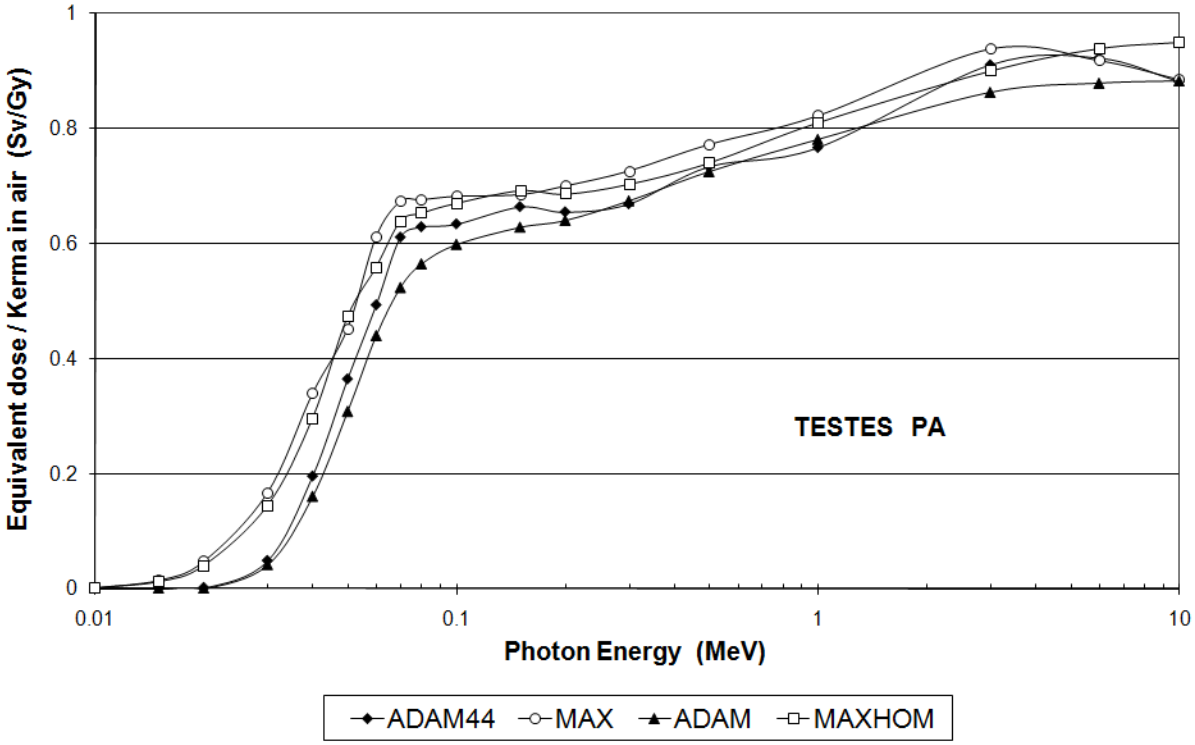

Figure 9b. Conversion coefficients for various phantoms between equivalent dose to the testes and air kerma free-in-air as a function of the incident photon energy for PA-incidence.

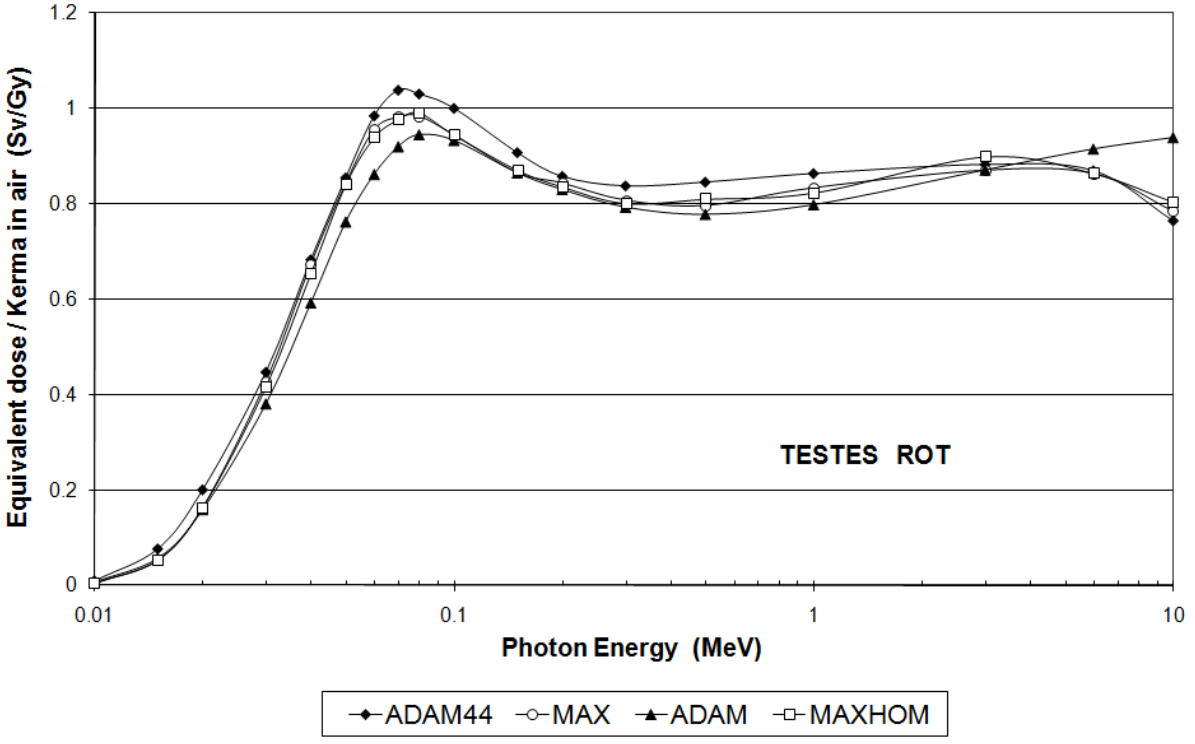

Figure 9c. Conversion coefficients for various phantoms between equivalent dose to the testes and air kerma free-in-air as a function of the incident photon energy for ROT-incidence.

Anatomy (ADAM44→MAXHOM)
The thighs of the ADAM44 phantom are closed, while those of the MAXHOM phantom are separated, as figures 1 and 3 show. As a consequence the ADAM44 testes receive more backscattered radiation for AP-incidence than the MAXHOM testes, and on the other hand less unattenuated radiation for PA-incidence because of the structural shielding by the thighs. The CCs reflect these anatomical differences.

Heterogeneous skeleton (MAXHOM→MAX)
No change to be observed within the margins of the coefficients of variance.

Red bone marrow (RBM)

Tissue composition (ADAM→ADAM44)
The RBM equivalent dose results from a complex superposition of various factors:
Figure 7 shows that the increase of skeletal calcium form 9.9% to 11.3% increases the RBM equivalent dose, and so does also the greater MEA coefficient of the ADAM44 phantom. On the other hand the new photoelectron correction factors from King and Spiers (1985) normally decrease the RBM equivalent dose compared to the ADAM data for all bones, except for the skull. Finally the change of the RBM mass fractions per bone from the ICRP23 based data to the ICRP70 based values has an increasing or decreasing effect on the RBM equivalent dose, depending on the direction of radiation incidence and the particular bone under consideration. Figures 10a-c show that the net result of this superposition are ADAM44 RBM CCs, which are generally greater than the RBM CCs for the ADAM phantom. At 70 keV the difference is 5% for AP-incidence, and 6% for PA-incidence, which agrees quite well with the 7% difference indicated by figure 7.

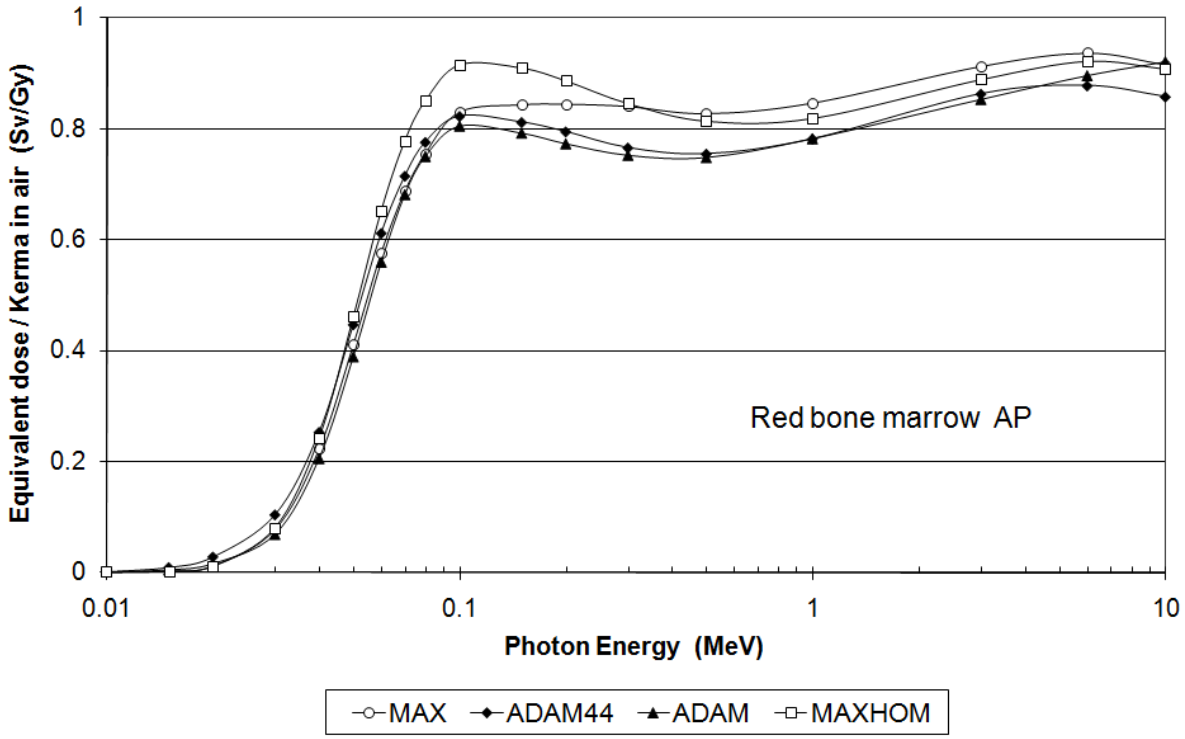

Figure 10a. Conversion coefficients for various phantoms between equivalent dose to the red bone marrow and air kerma free-in-air as a function of the incident photon energy for AP-incidence.

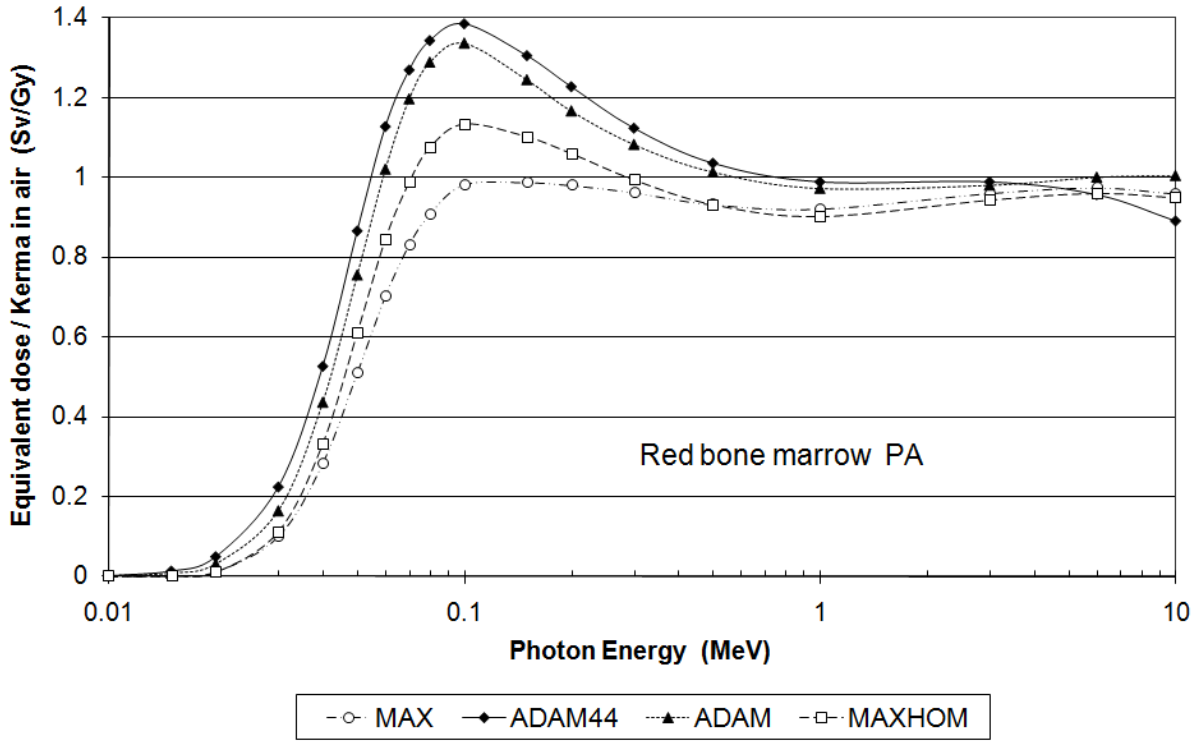

Figure 10b. Conversion coefficients for various phantoms between equivalent dose to the red bone marrow and air kerma free-in-air as a function of the incident photon energy for PA-incidence.

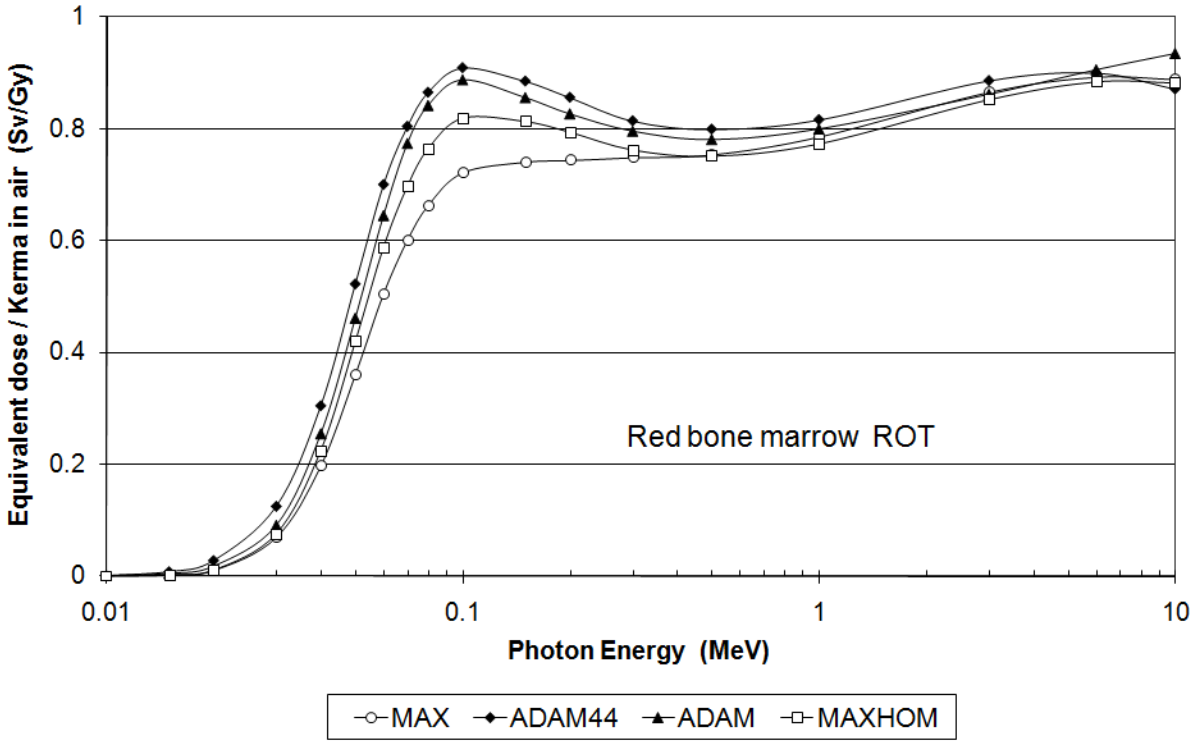

Figure 10c. Conversion coefficients for various phantoms between equivalent dose to the red bone marrow and air kerma free-in-air as a function of the incident photon energy for ROT-incidence.

Anatomy (ADAM44→MAXHOM)
As the same RBM model is applied to both phantoms, the differences of the CCs clearly reflect the different anatomies of the skeletons. Figures 1 and 4 show that compared to the ADAM44 skeleton, the spine, the pelvis, and the ribcage of the MAXHOM phantom are positioned more towards the front of the trunk. This fact explains the differences between the ADAM44 and MAXHOM RBM CCs demonstarted in figures 10a-c.

Heterogeneous skeleton (MAXHOM→MAX)
The RBM models of all phantoms considered here have one property in common, namely that the RBM equivalent dose is first of all a quantity derived from the equivalent dose to a homogeneous skeletal mixture. After that the RBM mass fractions, and the corrections factors may differ, and the homogeneous skeletal mixture may refer to one voxel, as in the case of the MAX phantom, or to a complete bone, as in the case of all other phantoms.
The average density of the MAX skeleton is 1.435 gcm^{-3}, and its average calcium content is 10.2% (Kramer et al 2003), which according to figure 7 would result in a 5% lower RBM equivalent dose compared to the MAXHOM RBM equivalent dose for 11.3% of calcium. But the MAX skeleton as a whole is not homogeneous, only the mixture per skeletal voxel is homogeneous. As an example, the average density of the MAX spine, which contains 42.6% of the total RBM mass, is 1.31 gcm^{-3}. This corresponds to ca. 7.2% of calcium, which according to figure 7 would reduce the RBM equivalent dose by ca. 23% compared to the value for 11.3% of calcium, which is the MAXHOM value. Other bones of the MAX phantom have different average densities or calcium contents, and different RBM mass fractions. The combined effect from all MAX bones which contribute to the RBM equivalent dose leads to the CCs shown in figures 10a-c, which are usually smaller than the CCs for the MAXHOM phantom.

Lungs

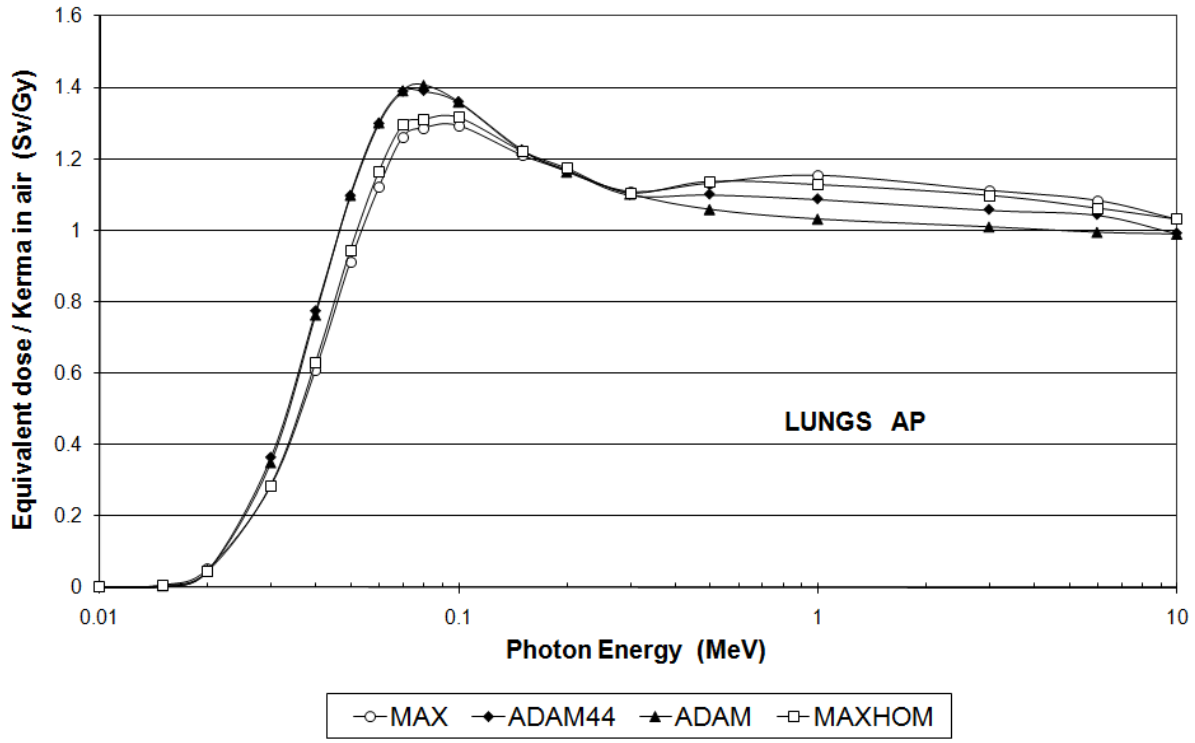

Figure 11a. Conversion coefficients for various phantoms between equivalent dose to the lungs and air kerma free-in-air as a function of the incident photon energy for AP-incidence

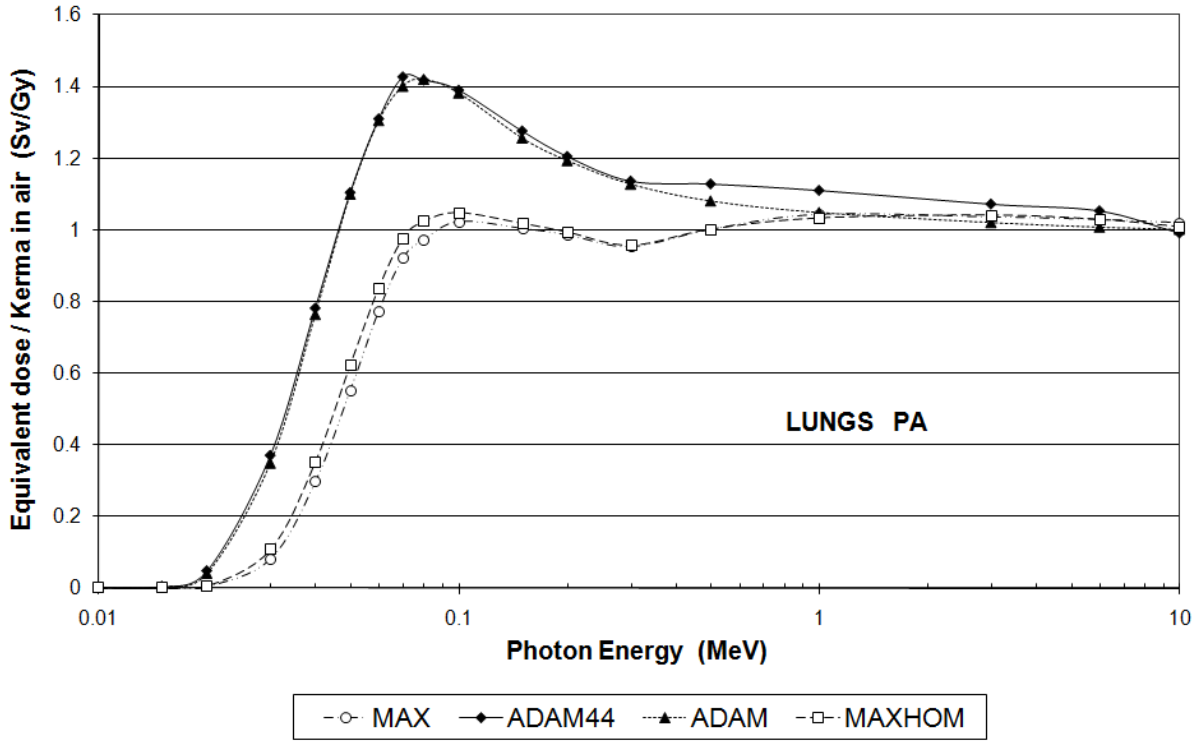

Figure 11b. Conversion coefficients for various phantoms between equivalent dose to the lungs and air kerma free-in-air as a function of the incident photon energy for PA-incidence.

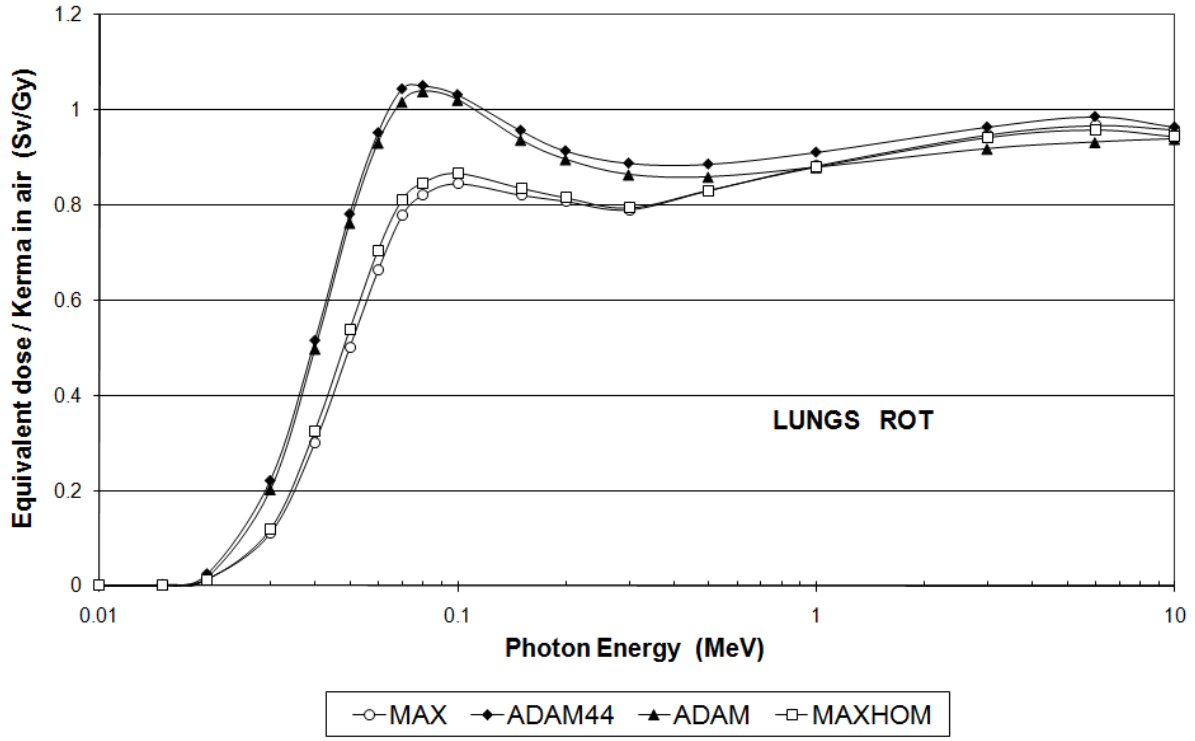

Figure 11c. Conversion coefficients for various phantoms between equivalent dose to the lungs and air kerma free-in-air as a function of the incident photon energy for ROT-incidence.

Tissue composition (ADAM→ADAM44)
According to figure 6 the lungs equivalent dose does not change because of the replacement of the lungs tissue (effect A). But effects B and C do have influence on the lungs equivalent dose, but they cancel each other out: Increased compositional shielding by the ribs equals reduced compositional shielding by the adipose/muscle mixture as figures 11a-c show.
Above 300 keV the ADAM44 lungs equivalent dose starts to exceed the ADAM lungs equivalent dose, because of the range of secondary electrons released in the bones of the ribcage, which increasingly deposit their energy in the lungs tissue. For very high incident photon energies this difference decreases because of the increasing range of the secondary electrons.

Anatomy (ADAM44→MAXHOM)
All lungs equivalent doses for the MAXHOM phantom are significantly smaller than those for the ADAM44 phantom. Figures 1, 3, and 4 show that the natural anatomy of the rib cage causes more structural shielding than the equidistantly spaced elliptical tori without sternum.

Heterogeneous skeleton (MAXHOM→MAX)
For the lungs the MAX CCs are smaller than the MAXHOM CCs because the average density of the MAX ribcage is 11% greater than the average density of the MAXHOM skeleton. This translates into ca. 16% calcium content, which according to figure 7 increases the compositional shielding for the lungs for photon energies below 300 keV.

3.4 Effective male dose

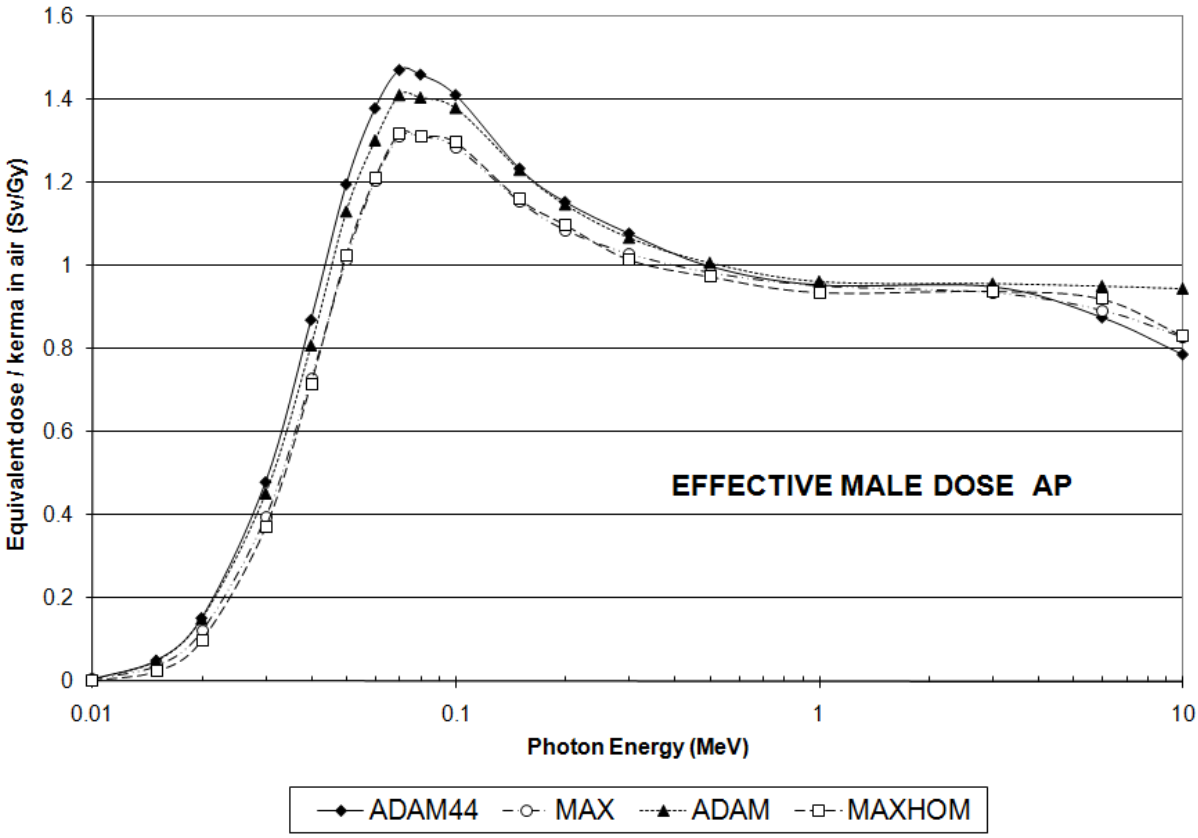

Figure 12a. Conversion coefficients for various phantoms between effective male dose and air kerma free-in-air as a function of the incident photon energy for AP-incidence.

Figures 12a-c show the effective male doses for the phantoms considered in this investigation. The findings for the organs and tissues discussed in the previous section are reflected in the CCs for the effective male dose:
The replacement of the tissue composition leads to an increase of the effective male dose (effects A-C), while the replacement of the anatomy causes a decrease of the effective male dose, due to depth-dose effects in extended organs, because of structural shielding from thicker layers of adipose and muscle, and because of the realistic human skeleton of the voxel phantom. The net effect from both replacements and from secondary electron effects at high energies causes a decrease of the effective male dose.
Figures 10a-c demonstrated that the introduction of a heterogenous skeleton led to a significant reduction of the RBM equivalent dose below 300 keV in the MAX phantom compared to the data for the MAXHOM phantom. In the effective male dose however the RBM equivalent dose has only a weight of 12% and therefore this reduction is less pronounced as figures 12a-c show. Additionally the low density of 1.31 gcm^{-3} of the MAX spine reduces for PA-incidence compositional shielding for radiosensitive organs, like the liver, the colon, and the stomach, which in turn increases the effective MAX dose.

Quantitative assessments of the dosimetric consequences of these replacements are shown in figures 13a-c. The replacement of the tissue composition is expressed by the ratio between the effective ADAM44 dose and the effective ADAM dose (ADAM44/ADAM), while the replacement of the phantom anatomy is quantified by the ratio between the effective MAXHOM dose and the effective ADAM44 dose (MAXHOM/ADAM44). At last the ratio between the effective MAX dose and the effective ADAM dose (MAX/ADAM) represents additionally the inclusion of a heterogeneous skeleton, and separately segmented volumes of adipose and muscle.

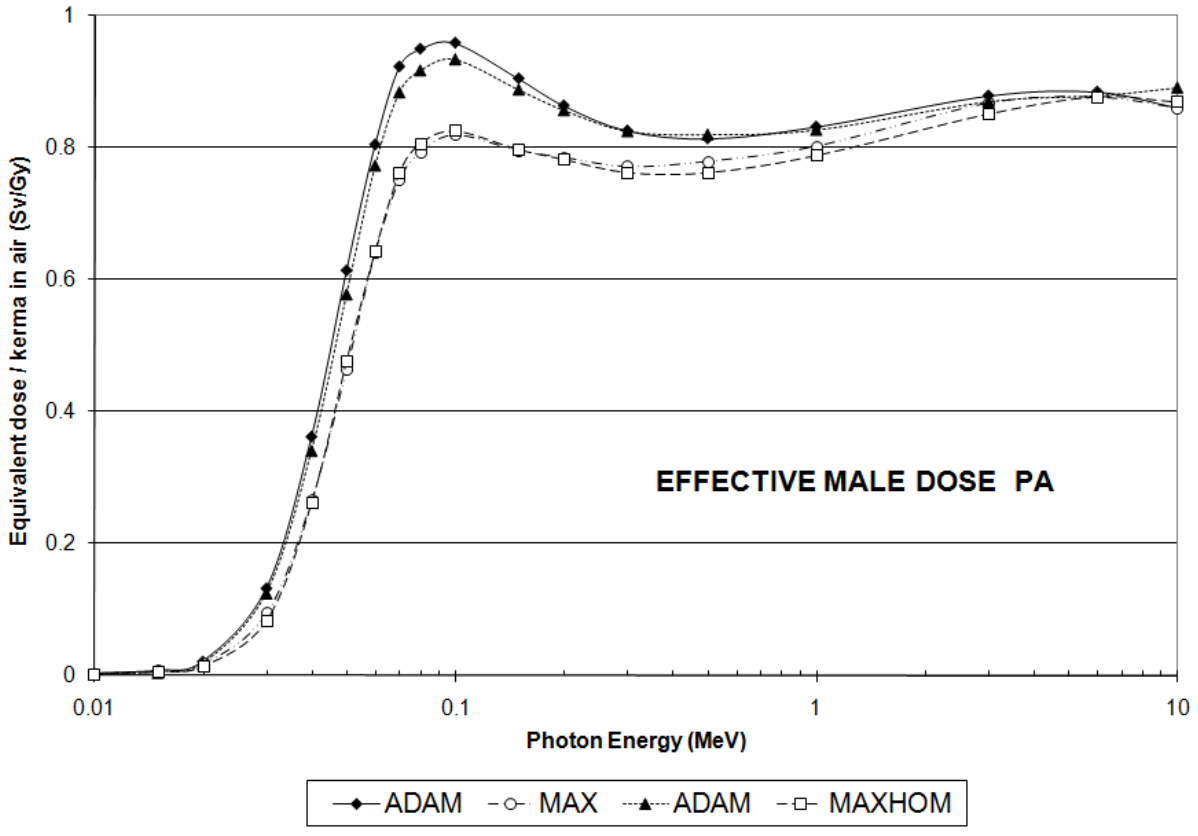

Figure 12b. Conversion coefficients for various phantoms between effective male dose and air kerma free-in-air as a function of the incident photon energy for PA-incidence.

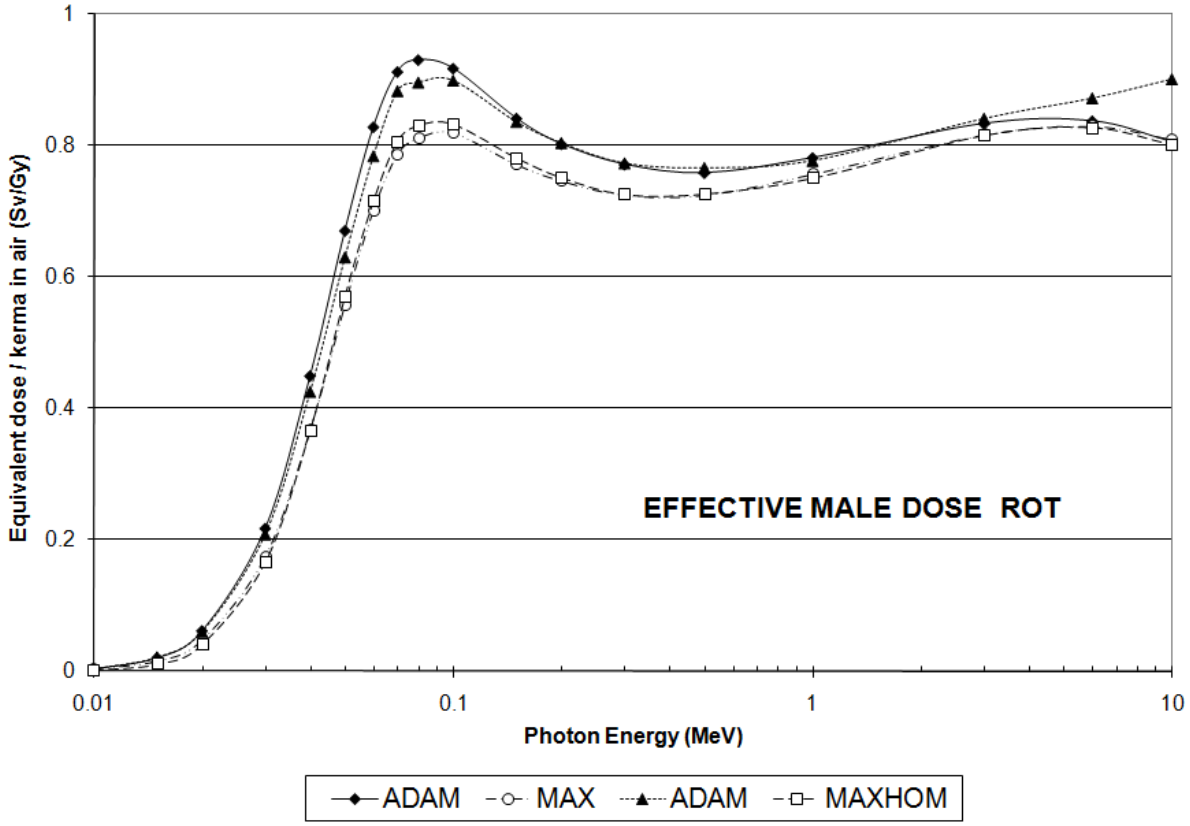

Figure 12c. Conversion coefficients for various phantoms between effective male dose and air kerma free-in-air as a function of the incident photon energy for ROT-incidence.

For incident photon energies below 30 keV for some organs the coefficients of variance show values of 20% and more, which leads to significant fluctuations of the effective male dose ratios as can be seen in figures 13a-c, but as their values are small anyway, they can be neglected for further considerations. Figures 13a-c indicate for photon energies above 30 keV that the replacement of the tissue compositions (ADAM44/ADAM) leads to an increase of the effective male dose by 10% at most, that the replacement of the phantom anatomy (MAXHOM/ADAM44) causes a decrease of the effective male dose by 38% at most, and that with the additional inclusion of a heterogeneous skeleton (MAX/ADAM) the maximum net difference between the effective MAX dose and the effective ADAM dose is 25%. For most incident photon energies and field geometries the differences are less than 15%.

3.5 Effective dose comparisons found in other investigations

Jones published two papers (1995, 1997) which, among other aspects, investigate also effective dose differences between the NORMAN voxel phantom (Dimbylow 1995) and the ADAM phantom for external exposure to photons for the field geometries mentioned above. The radiation transport code applied was the same for both phantoms, and so were the RBM model and the representation of the skeleton. For incident photon energies above 25 keV, and for AP-, PA-, and ROT-incidence Jones found a maximum difference of 8.3% for the replacement of the tissue composition, and a maximum difference of 22% for the replacement of the phantom anatomy.

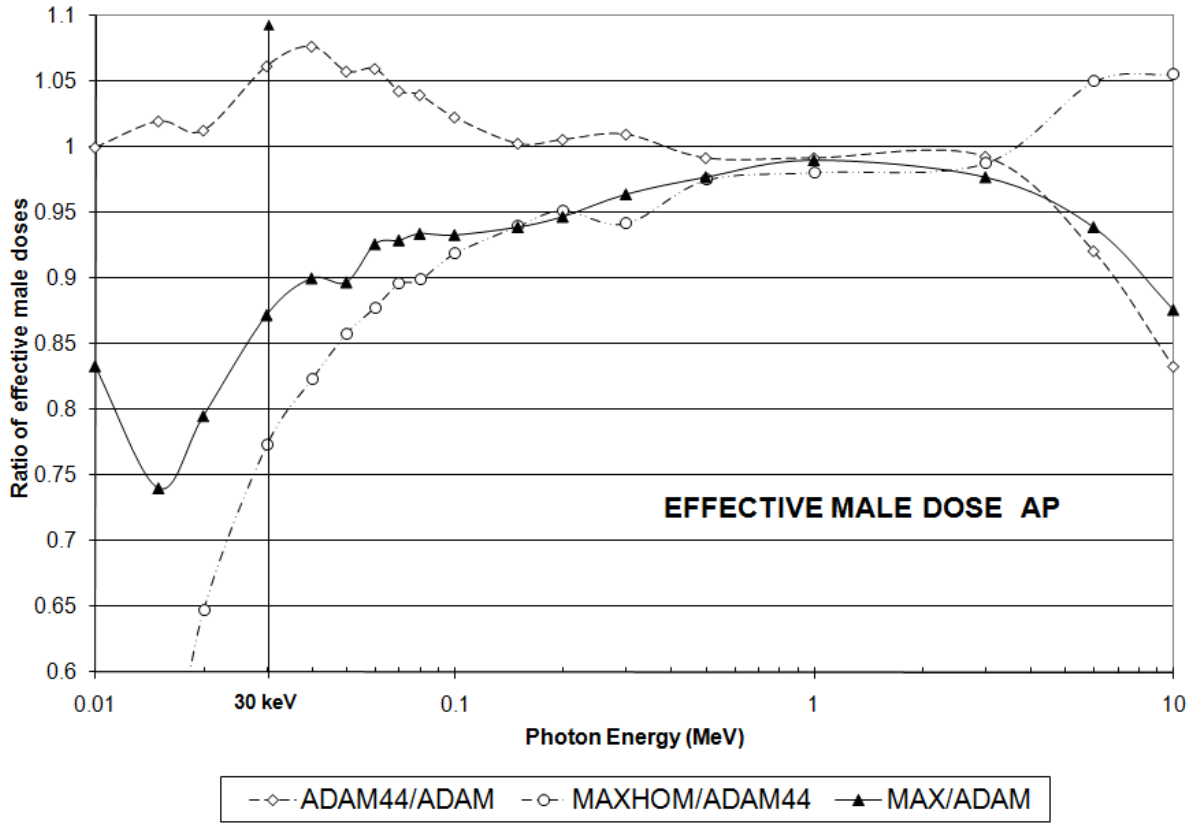

Figure 13a. Ratios of effective male doses as a function of the incident photon energy for AP-incidence for the replacement of the tissue composition (ADAM44→ADAM), for the replacement of the phantom anatomy (MAXHOM→ADAM44), and for the inclusion of a heterogeneous skeleton and segmented adipose and muscle (MAX→ADAM)

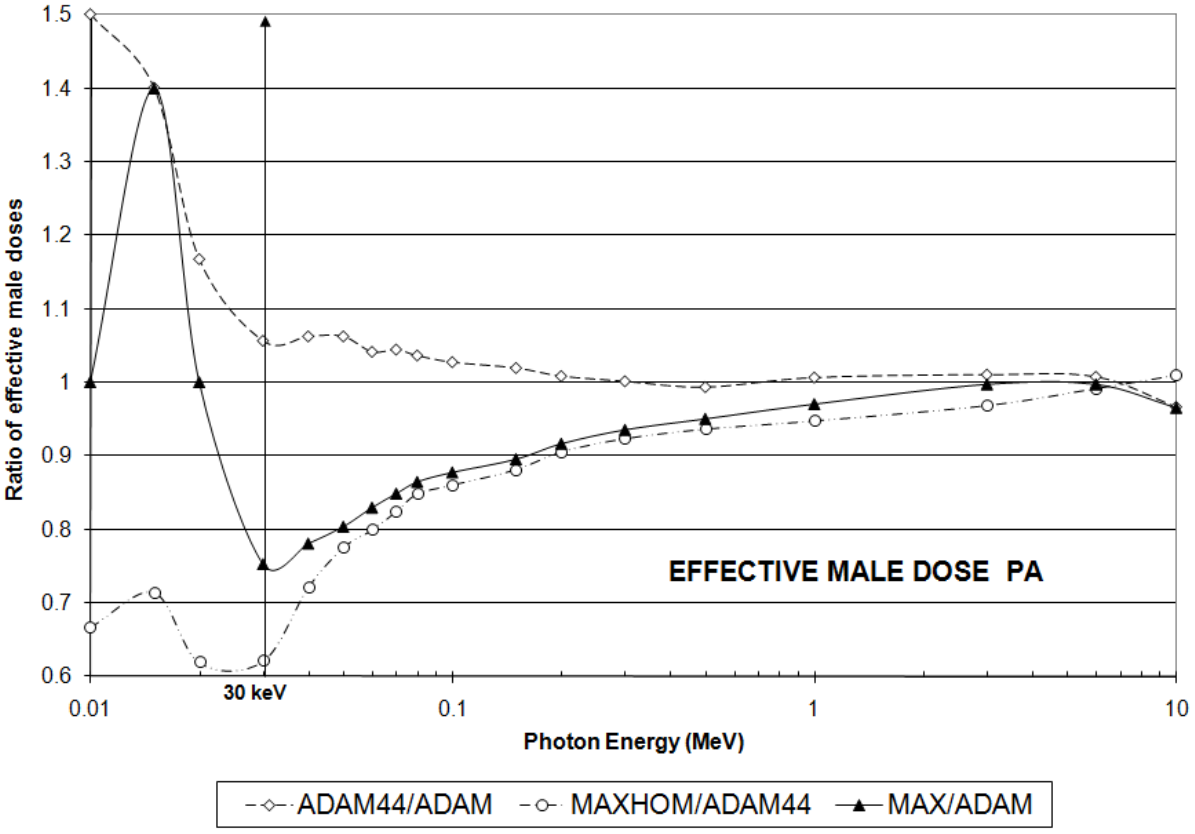

Figure 13b. Ratios of effective male doses as a function of the incident photon energy for PA-incidence for the replacement of the tissue composition (ADAM44→ADAM), for the replacement of the phantom anatomy (MAXHOM→ADAM44), and for the inclusion of a heterogeneous skeleton and segmented adipose and muscle (MAX→ADAM)

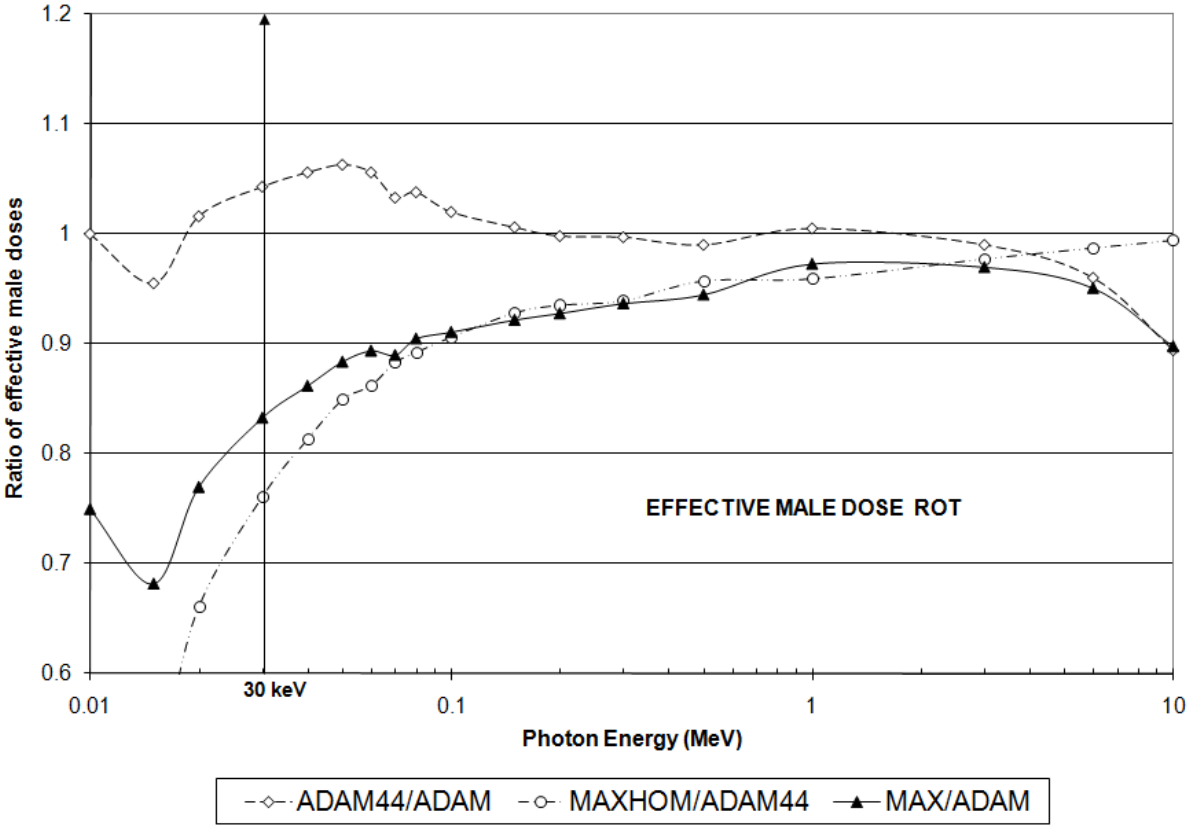

Figure 13c. Ratios of effective male doses as a function of the incident photon energy for ROT-incidence for the replacement of the tissue composition (ADAM44→ADAM), for the replacement of the phantom anatomy (MAXHOM→ADAM44), and for the inclusion of a heterogeneous skeleton and segmented adipose and muscle (MAX→ADAM)

Chao et al (2001) compared the effective VIP-MAN dose with the effective ADAM/EVA dose for external exposure to photons. Here not only were the two exposure models different with regard to the radiation transport code, to the tissue compositions, to the RBM model, and to the representation of the skeleton, but the two quantities to be compared were different too. The effective ADAM/EVA dose is a quantity averaged over both genders, while the effective VIP-MAN dose belongs to an adult male. For incident photon energies above 30 keV Chao et al found differences of up to 30% for AP-, and ROT-incidence, and up to 125% for PA-incidence.

Zankl et al (2002) published a comprehensive comparison of organ and tissue CCs for external photon exposures between a whole family of voxel phantoms, and the mathematical ADAM and EVA phantoms.
The radiation transport code applied was the same for all phantoms, the tissue compositions were different, and so were the RBM models and the representation of the skeleton. For incident energies above 30 keV Zankl et al found maximum differences of 20% between the effective voxel phantom doses and the effective ADAM/EVA dose.

4. Conclusions

The objective of this study was to investigate the dosimetric consequences if an exposure model based on a MIRD phantom is replaced by an exposure model based on a voxel phantom. Therefore the mathematical ADAM/GSF exposure model was systematically transformed into the voxel-based MAX/EGS4 exposure model. Step by step first the Monte Carlo code was replaced, then the compositions of the body tissues, then the phantom anatomy, and finally the tissue distribution in the skeleton, and the segmentation of adipose and muscle.

The results have shown that the replacement of the GSF Monte Carlo code by the EGS4 Monte Carlo code caused no significant changes of the organ and tissue equivalent doses.

The replacement of the elemental mass fractions of the body tissues led generally to an increase of soft-tissue organ equivalent doses, because absorption of radiation energy is greater in the ICRU44 soft-tissue compared to the ADAM soft-tissue (effect A). The replacement of the ADAM soft-tissue by the ADIMUS mixture in the unspecified regions of the ADAM phantom generally adds to the increase of organ equivalent dose due to reduced compositional shielding (effect B), while the opposite effect, namely a decrease of organ equivalent doses, is caused by greater compositional shielding by the new skeletal mixture (effect C).

In general the replacement of the ADAM anatomy by the MAX anatomy led to decrease of organ and tissue equivalent doses mainly because of

a) the anatomical structure of the realistic MAX skeleton (sternum, ribcage, pelvis) which, independent from its tissue composition, causes greater structural shielding for many internal organs compared to the ADAM skeleton,
b) the greater depth-dose effects in certain internal organs, the stomach for example, due to their realistic position, and especially their sometimes greater extension towards the rear part of the body, and
c) the increase of structural shielding by thicker layers of adipose and muscle.

At last the introduction of heterogeneously distributed skeletal tissues and of segmented regions between adipose and muscle can cause further reduction of equivalent dose for some organs and tissues depending on the bones in their vicinity. One can conclude that for given exposure conditions, tissue composition, and location the equivalent dose to an organ or tissue of the human body is basically a function of the compositional and structural shielding caused by the tissues in its vcinity.

The results show in particular that the effective male dose

a) changed up to 3% when the GSF code was replaced by the EGS4 Monte Carlo code,
b) increased up to 10% when the ADAM tissue compositions were replaced by ICRU44 based tissue compositions,
c) decreased up to 38% when the ADAM anatomy was replaced by the MAX anatomy, and
d) decreased up to 25% for the combined effect of a) to c), plus the inclusion of a heterogeneous skeleton and segmented regions for adipose and muscle.

Based on similar results found in the studies of Jones (1995, 1997) and of Zankl et al (2002), one can conclude that for external whole-body exposure to photons the replacement of the MIRD exposure models by voxel exposure models would reduce the adult effective male dose by up to 25%, for the majority of exposure situations considered here this value would not even reach 15%.

5. Acknowledgement

The authors would like to thank A. Bielajew, Michigan University, USA, and J. H. Hubbell, NIST, USA for many helpful discussions and support. The authors also would like to acknowledge the "Conselho Nacional de Desenvolvimento Científico e Tecnológico-CNPq" for the financial support.

6. References

Baro J, Sempau J, Fernandez-Varea J M and Salvat F 1995 PENELOPE: an algorithm for Monte Carlo simulation of the penetration and energy loss of electrons and positrons in matter Nucl.Instrum.Methods B **100** 31-46

Briesmeister J F 1997 MCNP – A general Monte Carlo N-Particle transport code, version 4B Los Alamos, NM, USA: Los Alamos National Laboratory; Report LA-12625-M

Chao T C, Bozkurt A and Xu X G 2001a Conversion Coefficients Based on the VIP-Man Anatomical Model and EGS4-VLSI Code for External Monoenergetic Photons from 10 keV to 10 MeV Health Physics 81(2):163-183

Chao T C, Bozkurt A and Xu XG 2001b Organ dose Conversion Coefficients for 0.1-10 MeV Electrons Calculated for the VIP-Man Tomographic Model Health Physics 81(2):203-214

Cristy M and Eckerman K F 1987 Specific Absorbed Fractions of Energy at Various Ages from Internal Photon Sources ORNL/TM-8381 Vol. 1-7,Oak Ridge National Laboratory, Oak Ridge, Tenn., USA

Dantas B M, Hunt J G, Spitz H B and Malatova I 2001 Physical vs Mathematical Anthropomorphic Phantoms: A Comparison between Real and Predicted Activities Proceedings of the 46th Annual Conference on Bioassay, Analytical, and Environmental Radiochemistry, 12.-17.11.2000, Seattle, WA, USA, http://www.lanl.gov/BAER-Conference/BAERCon-46p036.htm

Dimbylow, P J 1995 The development of realistic voxel phantoms for electromagnetic field dosimetry In: Proceedings of an International Workshop on Voxel Phantom Development held at the National Radiological Protection Board, Chilton, UK, 6-7 July

Hubbell J H and Overbo I 1979 Relativistic Atomic Form Factors and Photon Coherent Scattering Cross Sections J. Phys. Chem. Ref. Data 9, 69

Hunt J G, de S.Santos D, da Silva F C, Malatova I, Foltanova S, Dantas B M and Azeredo A 2000 Application of Voxel Phantoms and Monte Carlo Methods to Internal and External Dosimetry. Proceedings of the 10th Congress of the International Radiation Protection Association, IRPA10, 14.-19.5.2000, Hiroshima, Japan, http://www.irpa.net

ICRP 1975 Report of the Task Group on Reference Man ICRP Publication 23, International Commission on Radiological Protection, Pergamon Press, Oxford

ICRP 1991 1990 Recommendations of the International Commission on Radiological Protection. ICRP Publication 60 International Commission on Radiological Protection, Pergamon Press, Oxford

ICRP 1994 Dose coefficients for intakes of radionuclides by workers ICRP Publication 68, International Commission on Radiological Protection, Ann. ICRP, 24(4), Pergamon Press, Oxford

ICRP 1995 Basic Anatomical and Physiological Data for use in Radiological Protection: The Skeleton ICRP Publication 70.International Commission on Radiological Protection, Pergamon Press, Oxford

ICRP 1996 Conversion Coefficients for use in Radiological Protection against External Radiation ICRP Publication 74.International Commission on Radiological Protection, Pergamon Press, Oxford

ICRP 2002 2001 Annual Report of the International Commission on Radiological Protection http://www.icrp.org

ICRP 2003 Basic Anatomical and Physiological Data for Use in Radiological Protection: Reference Values Publication 89.International Commission on Radiological Protection, Pergamon Press, Oxford

ICRU 1989 Tissue substitutes in radiation dosimetry and measurement ICRU Report 44.International Commission on Radiation Units and Measurements, Bethesda, MD

ICRU 1998 Conversion coefficients for use in Radiological Protection against External Radiation. ICRU Report 57 International Commission on Radiation Units and Measurements, Bethesda, MD

Jones D G 1995 Use of voxel phantoms in organ dose calculations In: Proceedings of an International Workshop on Voxel Phantom Development held at the National Radiological Protection Board, Chilton, UK, 6-7 July

Jones D G 1997 A Realistic Anthropomorphic Phantom For Calculating Organ Doses Arising From External Photon Irradiation Radiation Protection Dosimetry Vol.72, No.1, pp. 21-29

Jones D G 1998 A realistic Anthropomorphic Phantom for Calculating Specific Absorbed Fractions of Energy from Internal Gamma Emitters Radiation Protection Dosimetry Vol.79, Nos.1-4, pp. 411-414

King S D and Spiers F W 1985 Photoelectron enhancement of the absorbed dose from X rays to human bone marrow: experimental and theoretical studies Br. J. of Radiol. **58**, 345-356

Kramer R 1979 Ermittlung von Konversionsfaktoren zwischen Körperdosen und Relevanten Strahlungskenngrößen bei Externer Röntgen- und Gamma-Bestrahlung Gesellschaft für Strahlen- und Umweltforschung, München-Neuherberg, GSF-Bericht-S-556

Kramer R, Zankl M, Williams G and Drexler G 1982 The Calculation of Dose from External Photon Exposures Using Reference Human Phantoms and Monte Carlo Methods. Part I: The Male (ADAM) and Female (EVA) Adult Mathematical Phantoms GSF-Report S-885.Reprint July 1999.Institut fuer Strahlenschutz, GSF-Forschungszentrum fuer Umwelt und Gesundheit, Neuherberg-Muenchen

Kramer R, Vieira J W, Khoury H J, Lima F R A and Fuelle D 2003 ALL ABOUT MAX: A Male Adult voXel phantom for Monte Carlo Calculations in radiation protection dosimetry Phys. Med. Biol. **48**, No.10, 1239-1262

Kramer R, Vieira J W, Khoury H J, Lima F R A 2004 **www.phantomax.org** (under construction)

Nelson W R, Hirayama H and Rogers D W O 1985 The EGS4 Code System SLAC-265 Stanford Linear Accelerator Center, Stanford University, Stanford, California

Petoussi-Henss N, Zankl M and Henrichs K 1997 Tomographic Anthropomorphic Models, Part III: Specific Absorbed Fractions of Energy for a Baby and a Child from Internal Sources GSF-Report 7/97. Institut für Strahlenschutz, GSF-Forschungszentrum für Umwelt und Gesundheit, München-Neuherberg

Petoussi-Henss N and Zankl M 1998 Voxel Anthropomorphic Models as a Tool for Internal Dosimetry Rad. Prot. Dos. Vol.79, Nos 1-4, pp. 415-418

Petoussi-Henss, N, Zankl M, Fill U and Regulla D 2002 The GSF family of voxel phantoms Phys. Med. Biol. 47:89-106

Roussin R W, Knight J R, Hubbell J H and Howerton R J 1983 Description of the DLC-99/HUGO package of photon interaction data in ENDF/B-V format Report No. ORNL-RSIC-46 (ENDF-335), Radiation Shielding Information Center, Oak Ridge National Laboratory, Oak Ridge, TN, USA

Saito K, Wittmann A, Koga S, Ida Y, Kamei T, Funabiki J and Zankl M 2001 Construction of a computed tomographic phantom for a Japanese male adult and dose calculation system Radiat Environ Biophys 40: 69-76

Smith T, Petoussi-Henss N and Zankl M 2000 Comparison of internal radiation doses estimated by MIRD and voxel techniques for a "family" of phantoms Eur J Nucl Med 27:1387-1398

Smith T, Phipps A W, Petoussi-Henss N and Zankl M 2001 Impact on Internal Doses of Photon SAFs Derived with the GSF Adult Male Voxel Phantom Health Physics, Vol. 80 No.5 pp

Snyder W S, Ford M R, Warner G G and Fisher H L 1969 Estimates of Absorbed Fractions for Monoenergetic Photon Sources Uniformly Distributed in Various Organs of a Heterogeneous Phantom MIRD Pamphlet No. 5, J. Nucl. Med. 10, Suppl. No. 3

Snyder W S, Ford M R, Warner G G and Watson G G 1974 Revision of MIRD Pamphlet No. 5 Entitled "Estimates of absorbed fractions for monoenergetic photon sources uniformly distributed in various organs of a heterogeneous phantom" ORNL-4979, Oak Ridge National Laboratory, Oak Ridge, Tenn.

Stabin M G and Yoriyaz H 2002 Photon Specific Absorbed Fractions Calculated in the Trunk of an Adult Male Voxel-Based Phantom Health Physics **82**(1): 21-44

Storm E and Israel H I 1970 Photon Cross-sections from 1 keV to 100 MeV for Elements Z=1 to Z=100 Atomic Data and Nucl. Tables 7, 565

Tagesson M, Ljungberg M and Strand S-E 1995 A computer program for the conversion of voxel based activity distribution to absorbed dose distribution in systemic radiation therapy In: Proceedings of an International Workshop on Voxel Phantom Development held at the National Radiological Protection Board, Chilton, UK, 6-7 July

Warner G G and Craig A M 1968 ALGAM: A Computer Program for Estimating Internal Dose for Gamma-Ray Sources in a Man Phantom Oak Ridge National Laboratory, Oak Ridge, Tenn., USA, Report ORNL-TM-2250

Xu X G, Chao T C and Bozkurt A 2000 VIP-MAN: An Image-based Whole-body Adult Male Model Constructed From Colour Photographs Of The Visible Human Project For Multi-particle Monte Carlo Calculations Health Physics 78(5):476-486

Xu X G and Chao T C 2003 Calculations of Specific Absorbed Fractions of the GI-Tract Using a Realistic Whole Body Tomographic Model Cancer Biotherapy and Radiopharmaceuticals (to be published)

Yoriyaz H, Santos A, Stabin M G and Cabezas R 2000 Absorbed fractions in a voxel-Based phantom calculated with the MCNP-4B code Med Phys 27(7)1555-1562

Zankl M, Drexler G, Petoussi-Henss N and Saito K 1997 The Calculation of Dose from External Photon Exposures Using Reference Human Phantoms and Monte Carlo Methods. Part VII: Organ Doses due to Parallel and Environmental Exposure Geometries GSF-Report 8/97. Institut für Strahlenschutz, GSF-Forschungszentrum für Umwelt und Gesundheit, München-Neuherberg

Zankl M, Panzer W and Herrmann C 2000 Calculation of Patient Doses Using a Human Voxel Phantom of Variable Diameter Rad. Prot. Dos. Vol.90, Nos1-2, pp 155-158

Zankl M and Wittmann A 2001 The adult male voxel model "Golem" segmented from whole-body CT patient data Radiat Environ Biophys 40: 153-162

Zankl M, Fill U, Petoussi-Henss N and Regulla D 2002 Organ dose conversion coefficients for external photon irradiation of male and female voxel models Phys Med Biol **47**, No.14, 2367-2386

Zubal I G, Harrell C R, Smith E O, Rattner Z, Gindi G and Hoffer P B 1994 Computerized three-dimensional segmented human anatomy Med.Phys.21 No.2, 299-302